Tree-partitioning Based Emergency Control for Mitigating Cascading Failures in Power Systems

Jian Xu, *Senior Member*, *IEEE*, Zhonghao He, Longwen Jia, Siyang Liao, *Member*, *IEEE*, and Yaokun Zou

***Abstract*—The emergency control strategy for mitigating cascading failures plays an important role in the safe and stable operation of power systems with high integration of renewable energy sources (RESs). To mitigate the high control costs associated with active splitting, this paper proposes a novel tree-partitioning based emergency control strategy. Initially, a coherency grouping model for power system integrated with wind turbines is established, incorporating an improved phase motion equation to facilitate the identification of unit homology. Furthermore, a modified fuzzy *c*-means (FCM) clustering algorithm is proposed to achieve the grouping of the generators. Then, the cluster partitioning issue is converted into an eigenvalue solution problem. This allows for a rapid and accurate cluster partitioning of the power system, taking into account both the random fluctuations of renewable energy output and the unit homology constraints. Based on the modified Prim's algorithm, the tree-partitioning method is used to select the optimal bridge, whereby other bridges are disconnected and the inter-cluster power imbalances remain stable. A power adjustment measure is proposed to determine the power adjustment amount within each cluster based on the power flow tracing. Simulations on the IEEE 118-bus system and the actual case system demonstrate that the proposed strategy reduces control costs by 55.60% and 43.26% compared with active splitting, while also accelerating the post-fault recovery. These results highlight the potential of the proposed strategy for mitigating cascading failures in real-world applications.**

***Index Terms*—Cascading failure, emergency control, tree-partitioning, cluster partitioning, coherency grouping, spectral clustering.**

Nomenclature

A. Sets and Indices

E	Set of edges in graph
G	Undirected weighted graph
i, j	Indices of generator nodes
n	Number of generators
O	Set of splitting nodes
O_d	Set of nodes in a different cluster from splitting nodes
T_{ij}	Index of coherency grouping of generator nodes i and j
V	Set of points in graph
V_T	Set of points in directly connected graph

B. Parameters

ω_0	Reference angular velocity of power system
λ_k	The k^{th} characteristic value of characteristic equation
δ_s	Initial phase angle of stator voltage vector
δ_{pll}	q-axis initial phase angle in phase-locked loop (PLL) coordinate system
η_i	Number of other sample points whose Euclidean distance from $\boldsymbol{b}_i$ is less than rank of $\boldsymbol{u}_2$
μ, σ^2	Mean and variance of Beta distribution
μ_{pl}, δ_{pl}	Expected value and variance of power load
A_{rv}^{-1}, A_{fw}^{-1}	Inverse elements of reverse and forward distribution matrices
a, b	Shape parameters of Beta distribution
$B(a,b)$	Beta distribution function
$\boldsymbol{b}_i$	The i^{th} matrix sample point
B_{ij}	Imaginary part of element from contracted node admittance matrix between generator nodes i and j
B_{jw}	Imaginary part of mutual admittance between generator node j and wind farm node w
$\boldsymbol{C}$	Cluster center matrix
C	Cut in graph partitioning
$\boldsymbol{D}$	Damping coefficient matrix of generator nodes
D_i	Damping coefficient of generator node i
D_w	Damping coefficient of power system for wind farm node w
E_i	Post-transient reactance voltage of generator node i
E_{ij}	Expected value of power flow for line ij
E_T	Active power in corresponding line
f_i	Element corresponding to the second smallest eigenvalue in characteristic equation of generator node i

Manuscript received: June 4, 2025; revised: September 29, 2025; accepted: November 4, 2025. Date of CrossCheck: November 4, 2025. Date of online publication: November 25, 2025.

This work was supported by National Natural Science Foundation of China (No. U22B6006).

J. Xu, Z. He, L. Jia (corresponding author), S. Liao, and Y. Zou are with the School of Electrical Engineering and Automation, Wuhan University, Wuhan, China, and Z. He is also with Yichang Power Supply Company, State Grid Hubei Electric Power Company, Yichang, China (e-mail: xujian@whu.edu.cn; hezhonghao@whu.edu.cn; 2294683296@qq.com; liaosiyang@whu.edu.cn; yaokunzou@whu.edu.cn).

DOI: 10.35833/MPCE.2025.000486

G_i	Subgraph with respect to graph G containing l independent subsets G_1, G_2, ..., G_l
$\bar{G}_i$	Supplement of G_i
G_{ij}, B_{ij}	Real and imaginary parts of admittance matrix between generator nodes i and j
G_{ij}^v	Utilization coefficient of generator node v on line ij
H_j	Inertia time constant of generator node j
$\boldsymbol{I}$	Unit matrix
i_{ds}	d-axis stator current
$\boldsymbol{K}$	Synchronizing power matrix of generator nodes
K_{ii}, K_{ij}	Self-synchronous power coefficient of generator node i and mutual-synchronous power coefficient between generator nodes i and j
K_{p}, K_{i}	Proportional and integral gains in proportional-integral (PI) control of PLL
L_{ij}^z	Utilization coefficient of load node z on line ij
$\boldsymbol{L}$	Unnormalized Laplacian matrix
$\boldsymbol{M}$	Inertia matrix of generator nodes
M_i	Inertia of generator node i
M_w	Inertia time constant of power system for wind farm node w
N	Number of nodes in graph G
N_{c}	Normative cut criterion
Q	Degree of node adjustment domain
$r_{\min}$	The 15$^{\text{th}}$ percentile value of density (defined as the minimum value) within all elements of $\boldsymbol{u}_2$
r_{wj}	Element related to frequency relationship between wind farm node w and generator node j
s_{r}	Slip ratio
$\boldsymbol{S}_0$, $\boldsymbol{T}_0$	Sensitivity matrices of node voltage and line power flow
T_{ij}	Coherent grouping index of generator nodes i and j
$T_{\mathrm{r}}(\cdot)$	Trace function
T_{th}	Threshold of coherent grouping
t_{ij}, b_{ij}	Transformer turn ratio and shunt admittance of line ij
$\boldsymbol{U}$	Node voltage vector
$\boldsymbol{U}_0$, $\boldsymbol{V}_0$	Voltage and power vectors at operating point
$\boldsymbol{u}_2$	The second eigenvector of characteristic equation
U_{s}	Amplitude of stator voltage vector
$\boldsymbol{V}$	Vector of active or reactive power flows of lines
V_i	Voltage at generator node i
w_{ij}	Weight of edge e_{ij} in graph G
$\boldsymbol{W}$	Weighted adjacency matrix

C. Variables

$\Delta\delta_i$	Power angle variation of generator node i
$\Delta\delta_{\mathrm{s}}$	Phase variation of stator voltage vector
$\Delta\delta_{\mathrm{pll}}$	Phase angle variation of PLL
$\Delta\omega_{\mathrm{pll}}$	Rotational angular velocity variation of PLL
$\Delta\boldsymbol{F}$	Random fluctuation of node-injected power relative to reference point
$\Delta\boldsymbol{F}^h$	The h^{th} order cumulant of node injection power
$\boldsymbol{G}_0$	Matrix of first-order partial derivatives of line power with respect to node voltage
$\boldsymbol{J}_0$	Jacobian matrix of power flow calculation
$P_{\mathrm{g}i}$, $Q_{\mathrm{g}i}$	Active and reactive power of generator node i
P_{F_j}	Active line power flow of generator node i
P_i	Active power flowing into generator node i
P_{ij}, Q_{ij}	Active and reactive power flows from generator nodes i to j
P_{l}	Load power in probability density function
$P_{\mathrm{l}i}$, $Q_{\mathrm{l}i}$	Active and reactive power of load at generator node i
P_{wpp}	Electromagnetic power of wind power plant
$\Delta P_{\mathrm{g}i}$	Electromagnetic power increment of generator node i
ΔP_{e}	Electromagnetic power variation of generator
ΔP_{m}	Mechanical power variation of generator
$\Delta\boldsymbol{U}^h$, $\Delta\boldsymbol{V}^h$	The h^{th} order cumulant for node voltage and line power flow

I. Introduction

THE power system in China will be characterized by a high integration of renewable energy sources (RESs), the widespread use of power electronic devices, and an extensive deployment of ultra-high-voltage (UHV) long-distance transmission infrastructure. The characteristics and dynamic behavior of cascading failures will be significantly influenced by the variability of RES output and the limited fault tolerance of power electronic equipment [1].

Unlike conventional power systems, the interactions between wind turbines (WTs) and conventional synchronous generators cause variations in transient voltage and power angle during faults. These changes in generator groupings can lead to incorrect identification of generators, affecting the optimal splitting solution. An inaccurate solution may lead to the widespread disconnection of generators and loads, jeopardizing the island stability and potentially triggering the disconnection of WTs, which could further result in disruptions across the power system [2], [3]. The primary goal of an emergency fault control strategy is to ensure the overall system safety, even if it requires sacrificing local stability. A key challenge in active network splitting is determining the optimal splitting boundary. Research in this area generally falls into three main categories of methods.

The first category of methods is based on slow coherency theory, which examines the dynamic behavior of the power system to identify weak connections between areas in real time. By identifying these weakly connected areas, these methods focus on finding splitting boundaries within the areas [4]-[6]. Although traditional slow coherency method can significantly reduce the solution scale, it fails to take into account the interaction effects between RES units and traditional units, resulting in inaccurate identification of the coordinated units and subsequently affecting the determination of the optimal solution.

The second category of methods is based on an intelligent optimization algorithm. References [7] and [8] employ optimization algorithms such as ant colony optimization to determine islanding schemes that maintain the power balance and prevent line overloading within the island. These algorithms also consider safety constraints such as power balance, dynamic stability, and synchronized island operation, accelerating the detection of splitting boundary. However, intelligent optimization algorithms require complex and time-consuming computations. As power systems grow in size and complexity, it becomes increasingly challenging to meet the computational speed requirement for real-time applications.

The third category of methods is based on graph theory. By simplifying and partitioning the network, these methods reduce the complexity of power system topology and improve the efficiency of determining optimal splitting boundaries [9], [10]. The calculations are primarily based on deterministic power flow, neglecting the effects of the uncertainty of RES output on the feasible solution space.

However, as an emergency control strategy to deal with cascading failures, active splitting inevitably disrupts the supply-demand balance within the power system, resulting in additional economic losses. Furthermore, after active splitting, the isolated islands must resynchronize before reconnecting to the power system, significantly increasing both the recovery time and black-start costs. Tree-partitioning has been proposed as a more conservative emergency failure control strategy [11]. In contrast to active splitting, the tree-partitioning method allows for power exchange between clusters, thereby reducing the requirement for strict supply-demand balance. Yet, conventional tree-partitioning based emergency control strategies fail to account for the dynamic characteristics of RES units or their effect on the clustering outcomes, as well as the unpredictable variations in RES output and load demand.

Building on the above analysis and acknowledging both the significant inaccuracies in traditional generator grouping methods and the variability of RES output, this paper proposes a novel tree-partitioning based emergency control strategy designed to mitigate cascading failures while minimizing control costs. The main contributions of this paper are described as follows.

1) An improved phase motion equation, reflecting the coherence characteristics of doubly-fed induction generators (DFIGs), is developed to create a new coherency grouping model for power system with integration of WTs. By proposing a modified fuzzy *c*-means (FCM) clustering algorithm, the grouping of different types of WTs and traditional generators is achieved.

2) A tree-partitioning method that considers the integration of WTs is proposed based on the modified Prim's algorithm. By applying graph theory, the complex cluster partitioning issue is effectively simplified.

3) A novel tree-partitioning based emergency control strategy is presented, which preserves the minimum connections between clusters. The proposed strategy aims to minimize the impact of lines by identifying the optimal disconnection schemes between clusters.

The remainder of this paper is organized as follows. Section II introduces the coherency grouping model for power system with integration of WTs. Section III analyzes the tree-partitioning method based on the modified Prim's algorithm. Section IV examines the proposed strategy. Section V presents a case study using the IEEE 118-bus power system and the actual case system to validate the proposed strategy. Finally, Section VI concludes this paper.

II. Coherency Grouping Model with Integration of WTs

A. Slow Coherency Theory

Traditional coherency theory based on the rotor motion equations of synchronous generators uses state variables associated with electromechanical oscillations in generator units as the key indicators for identifying coherent generator clusters [12]. The slow coherency theory presented here proceeds through the following procedures.

1) The power system topology is simplified, where the load is modeled as a constant impedance, and the generator node voltage is represented by the internal potential after transient reactance.

2) The formulation of the system state equation is constructed. For the simplified power system topology, the electromechanical behavior at the equilibrium point is captured through the second-order rotor motion equations of the synchronous generators at each generator node:

$$\boldsymbol{M}\frac{\partial^2 \boldsymbol{x}}{\partial^2 t}=\boldsymbol{K}\boldsymbol{x}+\boldsymbol{D}\frac{\partial \boldsymbol{x}}{\partial t} \tag{1}$$

where $\boldsymbol{M}=\mathrm{diag}(M_1, M_2, ..., M_n)$; $\boldsymbol{x}=[\Delta\delta_1, \Delta\delta_2, ..., \Delta\delta_n]^{\mathrm{T}}$; and $\boldsymbol{D}=[D_1, D_2, ..., D_n]^{\mathrm{T}}$.

3) According to the linearized equation for the transmission power of generator in the simplified power system topology proposed in [13], the electromagnetic power increment of generator node i is calculated as:

$$\Delta P_{gi}=\sum_{j=1, j\neq i}^{n} E_i E_j B_{ij}\cos(\delta_i-\delta_j)(\Delta\delta_i-\Delta\delta_j) \tag{2}$$

The generator nodes i and j are assigned to the homogenous group if the coherency grouping index $T_{ij}\geq T_{th}$, or to the non-homogenous group if $T_{ij}<T_{th}$, thus addressing the coherency partition problem. T_{ij} is defined as:

$$T_{ij}=\frac{n\sum f_i f_j-\sum f_i\sum f_j}{\sqrt{\left[n\sum f_i^2-\left(\sum f_i\right)^2\right]\left[n\sum f_j^2-\left(\sum f_j\right)^2\right]}} \tag{3}$$

T_{ij} reflects the degree of homogeneity between generator nodes i and j. The coherency grouping index ranges between (−1, 1), where higher values indicate a greater degree of homogeneity.

As outlined in [14], the number of system groups is equal to that of the chosen eigenvectors plus one. The imaginary part of the eigenvector in (1) corresponds to the oscillation frequency, allowing the selection of $k-1$ modes with the lowest frequencies. The number of coherent groups k can then be calculated by:

$$\min \frac{\lambda_k}{\lambda_{k+1}} \quad k=2,3,\ldots,n \tag{4}$$

The second smallest eigenvector captures the initial phase of the power angle for each generator unit at the equilibrium point under low-frequency oscillation, reflecting the degree of homogeneity among the generator units. This highlights the need for further research into the integration of WTs.

B. Homogeneity Identification of Generator Units Incorporating Improved Phase Motion Equation

An improved phase motion equation is derived from the power control model of DFIG and the phase-locked loop (PLL) model. During a fault in the power system, significant oscillations in both the system frequency and power angle will occur, causing a response in the dynamic behavior of the PLL. By applying linearization around the equilibrium point, the transfer function between the phase variation of stator voltage vector and the phase angle variation of PLL can be described as:

$$\Delta\delta_{\mathrm{s}} = \frac{s^2+\omega_0 U_{\mathrm{s}} K_{\mathrm{p}} s + \omega_0 U_{\mathrm{s}} K_{\mathrm{i}}}{\omega_0 U_{\mathrm{s}} K_{\mathrm{p}} s + \omega_0 U_{\mathrm{s}} K_{\mathrm{i}}} \Delta\delta_{\mathrm{pll}} \tag{5}$$

where U_{s} and ω_0 are both set to be 1 p.u..

By substituting (5) into the electromagnetic power calculation formula of DFIG, the transfer function between the variation in the electromagnetic power of DFIG and the variation in the PLL phase angle can be obtained as:

$$\Delta P_{\mathrm{e}} = \frac{3}{2}(1-s_{\mathrm{r}}) i_{ds} \frac{-s^2}{K_{\mathrm{p}} s + K_{\mathrm{i}}} \Delta\delta_{\mathrm{pll}} \tag{6}$$

Given that the value of s_{r} is relatively small, the dynamic behavior of the slip ratio is neglected in this paper. Considering $\Delta\delta_{\mathrm{pll}} = \omega_0 \Delta\omega_{\mathrm{pll}}/s$, the conversion of $\Delta\delta_{\mathrm{pll}}$ to $\Delta\omega_{\mathrm{pll}}$ leads to the following equation:

$$\frac{K_{\mathrm{p}} s + K_{\mathrm{i}}}{\frac{3}{2} i_{ds} s}(-\Delta P_{\mathrm{e}}) = \Delta\omega_{\mathrm{pll}} \tag{7}$$

By drawing an analogy to the mathematical form of the rotor motion equation for a conventional synchronous generator, (7) can be reformulated as:

$$(-\Delta P_{\mathrm{e}} - D_w \Delta\omega_{\mathrm{pll}}) \frac{\frac{2}{3} K_i}{i_{ds} s} = \Delta\omega_{\mathrm{pll}} \tag{8}$$

Combining (7) and (8), we have:

$$D_w = \frac{K_{\mathrm{p}} \Delta P_{\mathrm{e}}}{K_{\mathrm{i}} \Delta\omega_{\mathrm{pll}}/s} = \frac{K_{\mathrm{p}} \Delta P_{\mathrm{e}}}{K_{\mathrm{i}} \Delta\delta_{\mathrm{pll}}} \tag{9}$$

Analogous to the mathematical form of a traditional synchronous generator, the self-synchronizing power coefficient of the DFIG can be defined as $\Delta P_{\mathrm{e}}/\Delta\delta_{\mathrm{pll}}$, depending on the output power of each generator unit and the parameters of the power system topology. The transfer function of the DFIG resembles that of a conventional synchronous generator, as illustrated in Fig. 1, allowing the use of traditional coherency grouping methods for generator units.

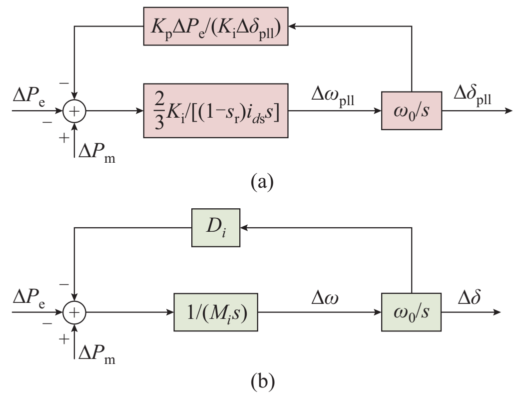

Fig. 1. Comparison of transfer functions of DFIG and conventional synchronous generator. (a) DFIG. (b) Conventional synchronous generator.

In terms of mathematical form, $D_w = K_{\mathrm{p}}\Delta P_{\mathrm{e}}/(K_{\mathrm{i}}\Delta\delta_{\mathrm{pll}})$ in the DFIG serves as a similar role to the damping coefficient D in synchronous generators, while $M_w = (1-s_{\mathrm{r}}) i_{ds}/(2K_{\mathrm{i}}/3)$ in the DFIG corresponds to the inertia time constant of a synchronous generator. Therefore, based on the homogeneity characteristic equation of synchronous generators, (8) is defined as the improved phase motion equation for the DFIG. This equation serves as the foundation for constructing a homogeneity identification model for generator units.

In order to reflect the real-world situation more accurately, this paper constructs a simplified power system with n generator nodes. Node i is connected to a wind farm consisting of m DFIGs, while the remaining $n-1$ generator nodes are equipped with synchronous generators. Assuming identical PLL parameters for all m DFIGs, the time-domain phase motion equation of the wind farm can be derived from (8) as:

$$\frac{(1-s_r) m i_{ds}}{\frac{2}{3}K_{\mathrm{i}}} \frac{\partial^2 \Delta\delta_{\mathrm{pll}}}{\partial^2 t} = -\Delta P_{\mathrm{wpp}} - \frac{\Delta P_{\mathrm{wpp}}}{\Delta\delta_{\mathrm{pll}}} \frac{K_{\mathrm{p}}}{K_{\mathrm{i}}} \Delta\omega_{\mathrm{pll}} \tag{10}$$

where the value of M_w for wind farms composed of m DFIGs is numerically equal to $m(1-s_{\mathrm{r}}) i_{ds}(2K_{\mathrm{i}}/3)$.

Assuming that the internal electric potential phasor of the wind farm is represented by $U_{\mathrm{s}}\angle\delta_{\mathrm{pll}}$, the self-synchronizing power coefficient K_{ii} and mutual synchronizing power coefficient K_{ij} of the wind farm can be expressed as:

$$\begin{cases} K_{ii} = -\sum\limits_{j=1, j\neq i}^{n} U_{\mathrm{s}} E_j B_{ij} \cos(\delta_{\mathrm{pll}} - \delta_j) \\ K_{ij} = U_{\mathrm{s}} E_j B_{ij} \cos(\delta_{\mathrm{pll}} - \delta_j) \end{cases} \tag{11}$$

From (11), $\boldsymbol{K}$ can be derived excluding the damping coefficient of generator from its elements. By substituting (10) and (11) into (1), the coherency grouping model with the integration of WTs can be obtained as:

$$\begin{bmatrix} M_1 & 0 & \ldots & 0 & \ldots & 0 \\ 0 & M_2 & \ldots & 0 & \ldots & 0 \\ \vdots & \vdots & & \vdots & & \vdots \\ 0 & 0 & \ldots & M_w & \ldots & 0 \\ \vdots & \vdots & & \vdots & & \vdots \\ 0 & 0 & \ldots & 0 & \ldots & M_m \end{bmatrix} \begin{bmatrix} \partial^2\Delta\delta_1/\partial^2 t \\ \partial^2\Delta\delta_2/\partial^2 t \\ \vdots \\ \partial^2\Delta\delta_{\mathrm{pll}}/\partial^2 t \\ \vdots \\ \partial^2\Delta\delta_n/\partial^2 t \end{bmatrix} = \boldsymbol{K} \begin{bmatrix} \Delta\delta_1 \\ \Delta\delta_2 \\ \vdots \\ \Delta\delta_{\mathrm{pll}} \\ \vdots \\ \Delta\delta_n \end{bmatrix} \tag{12}$$

As shown in (11) and (12), $\boldsymbol{K}$ is governed by the grid-connected capacity of the wind farm, the location of the connection point, and the grid topology. In contrast, M_w is determined by the stator current and PLL parameters. Through the matrix perturbation theory [15], the results of unit homology are simplified for calculation when PLL parameters are changed. Hence, the integration of WTs modifies the power flow and changes the parameters of the homogeneity identification model, thereby affecting the homogeneity of the generator units.

For other types of WTs, this paper focuses on the influence of their connection capacity and location on the synchronization characteristics, and the external characteristics of WT output can be equivalently represented as the conductance [16]. The equivalent inertia M_{ow} for other types of WTs is given as:

$$M_{\mathrm{ow}}=\frac{\sum_j B_{jw}}{\sum_j \frac{1}{H_j} r_{wj} B_{jw}} \tag{13}$$

The traditional FCM clustering algorithm randomly selects the initial clustering center, which is sensitive to the initial center point and easy to fall into local optimization. This paper modifies the traditional FCM clustering algorithm to improve the clustering quality. The modified FCM clustering algorithm is presented in Algorithm 1.

Algorithm 1: modified FCM clustering algorithm

1. **Input**: $\boldsymbol{u}_2$, k, $r_{\min}$
2. Calculate η_i of all sample points in $\boldsymbol{u}_2$. Find the center point c_1 corresponding to the maximum value of η_i. Put c_1 into $\boldsymbol{C}$, where $\boldsymbol{C}=[c_1, c_2, ..., c_k]$. Calculate the minimum distance D_i between each of the remaining sample points and all the center points in $\boldsymbol{C}$
3. Find $\boldsymbol{b}_i$ corresponding to the maximum value of D_i. If $\eta_i > r_{\min}$, $\boldsymbol{b}_i$ becomes the next center point and is put into $\boldsymbol{C}$; otherwise, search for other sample points in descending order
4. If the number of points in $\boldsymbol{C}$ equals k, the algorithm ends; otherwise, go to the second step
5. **End**

III. Tree-partitioning Method Based on Modified Prim's Algorithm

A. Stochastic Power Flow Based on Cumulant

The expected values derived from the stochastic power flow are utilized as the inputs to the spectral clustering algorithm detailed in Section III-B. With the growing integration of WTs in power systems, it is necessary to consider the impacts of WTs and load fluctuations. Therefore, the probability distribution functions for both WT output and load power are employed as the foundation for the subsequent stochastic power flow analysis.

Reference [17] demonstrates that the Beta distribution can be used to establish a suitable probabilistic model for wind farm output, employing the probability density function f_B defined as (14) with the bounded random variable $x \in [0, 1]$.

$$f_B(x; a, b)=\frac{1}{B(a, b)} x^{a-1}(1-x)^{b-1} \tag{14}$$

$$B(a, b)=\int_0^1 x^{a-1}(1-x)^{b-1} \mathrm{d}x \tag{15}$$

$$a=\frac{(1-\mu)\mu^2}{\sigma^2}-\mu \tag{16}$$

$$b=\frac{1-\mu}{\mu} a \tag{17}$$

For short-term load power prediction, current research indicates that the load power follows a normal distribution, and its probability density function in this case can be expressed as:

$$f(P_1)=\frac{1}{\sqrt{2\pi}\,\sigma_{P_1}} \mathrm{e}^{-\frac{(P_1-\mu_{P_1})^2}{2\sigma_{P_1}^2}} \tag{18}$$

For traditional deterministic power flow calculations, the Newton-Raphson method is commonly used to solve the equations. The equations in polar coordinates are expressed as:

$$\begin{cases} P_{\mathrm{g}i}-P_{\mathrm{l}i}-V_i \sum\limits_{j=1}^{N} V_k (G_{ij}\cos\delta_{ij}+B_{ij}\sin\delta_{ij})=0 \\ Q_{\mathrm{g}i}-Q_{\mathrm{l}i}-V_i \sum\limits_{j=1}^{N} V_k (G_{ij}\sin\delta_{ij}-B_{ij}\cos\delta_{ij})=0 \end{cases} \tag{19}$$

Similarly, the transmission power equations for the lines can be expressed in polar coordinates as:

$$\begin{cases} P_{ij}=-t_{ij}G_{ij}V_i^2+V_iV_j(G_{ij}\cos\delta_{ij}+B_{ij}\sin\delta_{ij}) \\ Q_{ij}=\left(t_{ij}B_{ij}-\dfrac{b_{ij}}{2}\right)V_i^2+V_iV_j(G_{ij}\sin\delta_{ij}-B_{ij}\cos\delta_{ij}) \end{cases} \tag{20}$$

The equations of node injection power and power flow of the lines in polar coordinates can be written in matrix form. By performing a Taylor series expansion of the power flow equations around the operating point and omitting higher-order terms, (21) and (22) can be obtained.

$$\begin{cases} \boldsymbol{U}=\boldsymbol{U}_0+\Delta\boldsymbol{U} \\ \boldsymbol{V}=\boldsymbol{V}_0+\Delta\boldsymbol{V} \end{cases} \tag{21}$$

$$\begin{cases} \Delta\boldsymbol{U}=\boldsymbol{J}_0^{-1}\Delta\boldsymbol{F}=\boldsymbol{S}_0\Delta\boldsymbol{F} \\ \Delta\boldsymbol{V}=\boldsymbol{G}_0\boldsymbol{J}_0^{-1}\Delta\boldsymbol{F}=\boldsymbol{T}_0\Delta\boldsymbol{F} \end{cases} \tag{22}$$

Based on the principle that the h^{th}-order cumulant of a random variable scaled by r is equal to r^h times the h^{th}-order cumulant of the variable [18], $\Delta\boldsymbol{U}^h$ and $\Delta\boldsymbol{V}^h$ can be expressed as:

$$\Delta\boldsymbol{U}^h=\boldsymbol{S}_0^h\Delta\boldsymbol{F}^h \tag{23}$$

$$\Delta\boldsymbol{V}^h=\boldsymbol{T}_0^h\Delta\boldsymbol{F}^h \tag{24}$$

After determining the h^{th}-order cumulant of node voltage and line power flow from (23) and (24), the probability distribution functions of the node voltage and line power flow can be obtained via the Gram-Charlier series expansion, facilitating the calculation of the expected power flow of each line [19].

B. Theoretical Foundations of Graph Partitioning

The subsection focuses on the cluster partitioning problem, aiming to identify the optimal partitioning while adhering to predefined constraints. In this paper, the power system is represented as $G=(V,E)$. The elements W_{ij} of $\boldsymbol{W}$, D_{ij} of $\boldsymbol{D}$, graph size $V_g(G)$, and $\boldsymbol{L}$ are defined as:

$$W_{ij}=\begin{cases} w_{ij} & E_{ij}\in E \\ 0 & E_{ij}\notin E \end{cases} \tag{25}$$

$$w_{ij}=\begin{cases} \dfrac{E_{ij}+E_{ji}}{2} & i\neq j \\ 0 & i=j \end{cases} \tag{26}$$

$$D_{ij}=\begin{cases} \sum\limits_{j} w_{ij} & i=j \\ 0 & i\neq j \end{cases} \tag{27}$$

$$V_g(G)=\sum_{i\in V} D_{ii} \tag{28}$$

$$\boldsymbol{L}=\boldsymbol{D}-\boldsymbol{W} \tag{29}$$

where E_{ij} is calculated using the stochastic power flow model in Section III-A, incorporating uncertainties in WT output and load power. Equations (25) and (27) reveal the connectivity and classification information within $\boldsymbol{W}$ of the graph. While multiple criteria have been proposed for graph partitioning, this paper focuses on the normalized cut criterion N_c, which is defined as.

$$N_c(G_1,G_2,...,G_l)=\sum_{i=1}^{l}\frac{C(G_i,\bar{G}_i)}{V_g(G_i)} \tag{30}$$

$$C(G_i,\bar{G}_i)=\sum_{i\in G_i, j\in \bar{G}_i} w_{ij} \tag{31}$$

Once the graph partitioning criterion is determined, the problem can be transformed into a problem of finding the minimum value of $N_c(G_1,G_2,...,G_l)$. This problem falls into the category of non-deterministic polynomial (NP) and is typically solved using spectral clustering algorithms.

C. Cluster Searching

In Section III-B, the normalized cut criterion is used to reformulate the graph partitioning problem as the minimization of $N_c(G_1,G_2,...,G_l)$. The Laplacian-based graph partitioning method constructs the Laplacian matrix from the initial graph and its adjacency matrix. Clustering is achieved by solving the eigenvalues and eigenvectors of this matrix. Let $\boldsymbol{H}$ be an $N\times l$ indicator matrix, where each element is defined as:

$$H_{ij}=\begin{cases} \dfrac{1}{\sqrt{V_g(G_j)}} & i\in G_j \\ 0 & i\notin G_j \end{cases} \quad i=1,2,...,N, j=1,2,\dots,l \tag{32}$$

Reference [20] shows that minimizing $N_c(G_1,G_2,\dots,G_l)$ is equivalent to the constrained optimization problem in (33).

$$\begin{cases} \min\limits_{G_1,G_2,...,G_l} T_r(\boldsymbol{H}^T\boldsymbol{L}\boldsymbol{H}) \\ \text{s.t. } \boldsymbol{H}^T\boldsymbol{D}\boldsymbol{H}=\boldsymbol{I} \end{cases} \tag{33}$$

The normalized Laplacian matrix is defined as $\boldsymbol{L}'_{rw}=\boldsymbol{D}^{-1}\boldsymbol{L}$, allowing $\boldsymbol{H}$ to be extended into the domain of real numbers. Rayleigh's theorem [21] has confirmed that $\boldsymbol{H}$ is composed of the eigenvectors associated with the smallest l eigenvalues. Therefore, clustering the row vectors of $\boldsymbol{H}$ produces the desired graph partitioning. This paper employs the modified FCM clustering algorithm shown in Algorithm 1.

The cluster searching takes into account the constraints of dividing generator units with integration of WTs by introducing constraint pairs: must-link (ML) and cannot-link (CL). The ML indicates that two nodes are assigned to the same region, while the CL indicates that two nodes are assigned to different regions. These constraints guide the clustering process to produce a division that satisfies the specified conditions. Detailed solution method can be found in [22].

IV. Proposed Strategy

A. Tree-partitioning Method

Assume a simple power system topology where clustering has been completed, and the six clusters are labeled as A-F. By treating each cluster as an individual entity, this paper creates a tree structure that represents the tree-partitioning, as shown in Fig. 2.

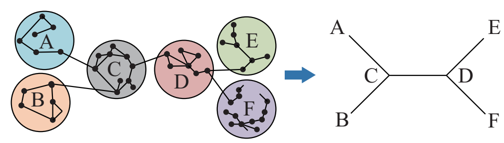

Fig. 2. Tree-partitioning of a simple power system topology.

The clusters are connected by bridges. References [23] and [24] have shown that line faults within a cluster do not affect the power flow distribution in other clusters, provided that inter-cluster power imbalances remain stable and the connecting bridges between clusters are preserved. The tree-partitioning method allows cascading failures to be contained at a local level.

B. Principle of Selecting Optimal Bridge

After applying the tree-partitioning method, the resulting clusters are interconnected by bridges. The key challenge then becomes selecting the optimal bridge in a way that ensures the system security and stability during cascading failures. To minimize disturbances from line disconnections, the principle of selecting the optimal bridge prioritizes minimizing the line impact. This is achieved by preferentially disconnecting lines with lower transmission power, while preserving those with higher transmission power. This paper employs a modified Prim's algorithm to identify the set of bridges with the maximum transmission power in a weighted connected graph [25]. The modified Prim's algorithm is presented in Algorithm 2.

C. Power Adjustment Measure

Unlike active splitting control, the tree-partitioning method retains bridges between clusters, enabling continued power exchanges. In this case, each cluster does not operate in the islanded mode.

Algorithm 2: modified Prim's algorithm

1. **Input**: transform the clusters and lines connecting the clusters into a directed connected graph $G_T=(V_T,E_T)$
2. Define the maximum spanning tree $MST=(U_M,T_M)$, where the sets of points and lines in MST are $U_M=\varnothing$ and $T_M=\varnothing$, respectively
3. Select any cluster $u_1\in V_T$ as the initial vertex, where $U_M=\{u_1\}$, $T_M=\varnothing$
4. For all the clusters $v_T\in V_T-U_M$, select the edge (u_1,v_T) with the maximum weight, add v_T to U_M, and add (u_1,v_T) to T_M
5. If $U_M=V_T$, go to the next step; otherwise, go to the previous step
6. **Output**: MST

In a cluster after splitting, the node connected to the disconnected line is defined as the splitting node M. The one-degree node adjustment domain consists of nodes directly connected to the splitting node by a single edge, excluding those belonging to other clusters. Similarly, the two-degree node adjustment domain includes nodes connected by a single edge to the one-degree nodes, again excluding nodes from different clusters. As the degree of the node adjustment domain increases, the electrical distance between the nodes and the splitting nodes also increases proportionally. The Q-degree node adjustment domain can be calculated by:

$$O^Q=f_s(O^{Q-1})-O_d \tag{34}$$

where f_s represents the searching process for the $(Q-1)$-degree node adjustment domain.

Equation (34) exhibits recursive properties, allowing the use of a breadth-first search algorithm to identify the adjustment domains for each degree of the splitting node. To minimize the scope of adjustment, this domain is typically restricted to a degree of no more than three.

The power flow tracing is based on the proportional sharing principle. It determines the distribution of power flow across lines by solving parameters related to lines, nodes, and the overall topology. The power flow tracing can be classified into forward or reverse tracing, depending on the direction of analysis. By using these two ways of power flow tracing, the line utilization coefficients for the generator and load nodes [26] can be defined as:

$$G_{ij}^{v}=\frac{\left|P_{ij}\right|+\left|P_{ji}\right|}{2P_i}A_{\mathrm{rv}}^{-1} \tag{35}$$

$$L_{ij}^{z}=\frac{\left|P_{ij}\right|+\left|P_{ji}\right|}{2P_j}A_{\mathrm{fw}}^{-1} \tag{36}$$

If the power adjustment required for line ij is ΔP_{ij}, the power adjustment required ΔP_{jk} for line jk that flows out from node j can be described as:

$$\Delta P_{jk}=\Delta P_{ij}\frac{P_{jk}}{\sum P_{F_j}} \tag{37}$$

After determining the power adjustments required for all lines connected to generator node j, (37) is iterated until the power adjustment for line ij is fully allocated to the corresponding load nodes and generator nodes. The adjustment quantity for the load nodes and generator nodes can then be obtained. To sum up, the flowchart of the proposed strategy is shown in Fig. 3.

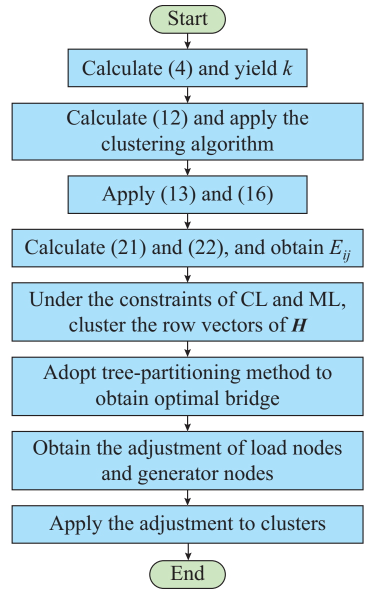

Fig. 3. Flowchart of proposed strategy.

V. CASE STUDY

The proposed strategy is verified to mitigate cascading failures on the IEEE 118-bus system as well as an actual case system, and the simulation step size is 20 μs in PSS/E. The wind power forecasting error follows a Beta distribution with a mean of 0.7 and a variance of 0.1, while the load follows a normal distribution with a standard deviation of 10% of its peak value.

The DFIG parameters are set to align with those of the WT3 model in PSS/E, with the PLL parameter K_i set to be 333. The adjustment cost is 2 \$/MW for generator dispatch control, 30 \$/MW for generator curtailment, and 100 \$/MW for load shedding [27], respectively. The program is developed using MATLAB R2021a and runs on a personal computer with Intel-i5-12400-2.5 GHz CPU and 8 GB of memory.

A. Coherency Identification of Generator Groups with Integration of WTs

The topology of the IEEE 118-bus system includes 19 generators, which is shown in Fig. 4.

In Fig. 4, buses 10, 12, and 25 are replaced by wind farms with equivalent generation capacity, leading to a penetration rate of WTs of approximately 17%. After solving the coherency grouping model in (12), the normalized per-unit values of the elements related to the second eigenvalue of the system are represented by the yellow line in Fig. 5. In order to make comparisons with other methods, this paper sets the fault scenario as a three-phase-to-ground fault occurs on line 38-65, with fault clearance after 0.1 s. The normalized steady-state per-unit values of phase angles using the Fourier analysis [28] in this scenario are shown by the green line in Fig. 5.

The per-unit values of generator group elements are clustered using the modified FCM clustering algorithm. The clustering results are {G1-G14}, {G15}, {G16-G19}, which means that the coherency grouping model has the same grouping results as the Fourier analysis, further confirming its accuracy and reliability.

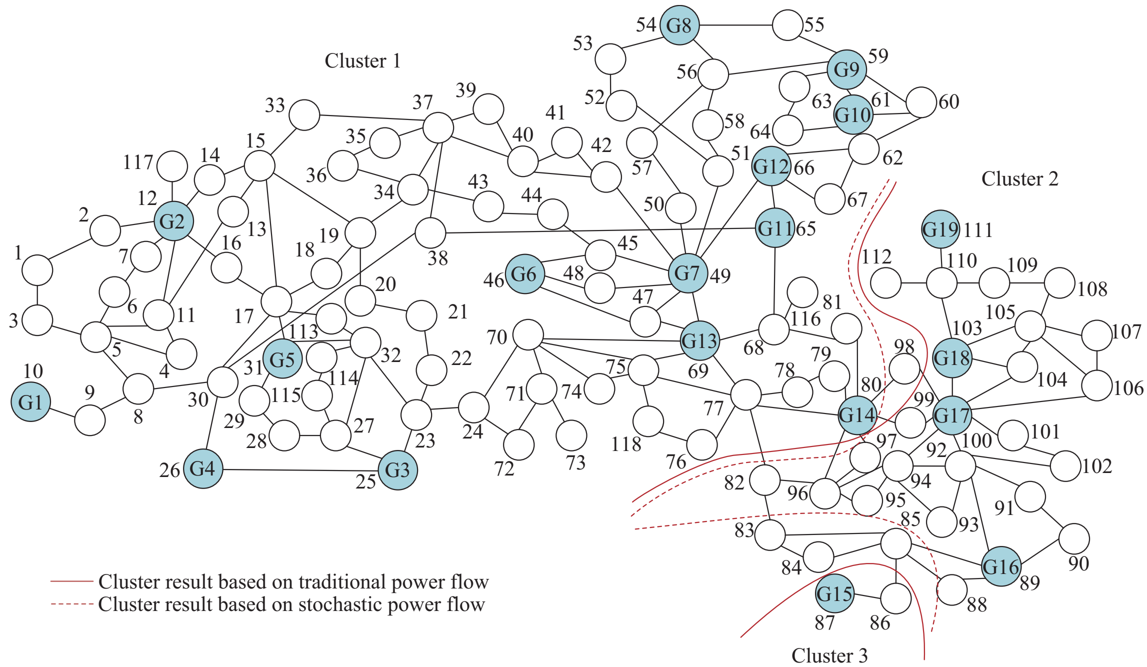

Fig. 4. Topology of IEEE 118-bus system.

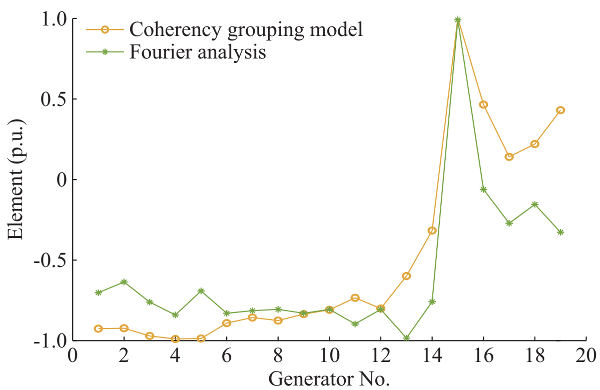

Fig. 5. Comparison results of elements related to the second eigenvalue of system.

Unlike the Fourier analysis, the coherency grouping model is immune to measurement errors in electrical quantities [29]. Meanwhile, it allows for offline calculation of grouping results and supplies detailed analytical expressions.

To validate the necessity of the coherency grouping model, the same fault is simulated in the conventional system and the system with 10% penetration rate of WTs. The fault conditions are set as follows: a three-phase-to-ground fault occurs on line 38-65 at 0.1 s, followed by the faulty line disconnection at 1.1 s. The rotor angular velocity curves of each generator in different power systems are presented in Fig. 6.

As shown in Fig. 6, the clustering results in the traditional power system are {G1-G5}, {G6-G14}, {G15-G19}, while the clustering results in the power system with the integration of WTs are {G1-G14}, {G15}, {G16-G19}. The above results can be explained from the following two aspects.

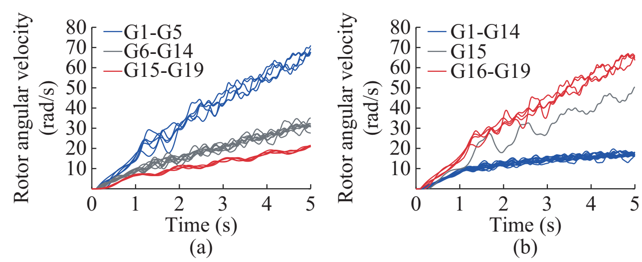

Fig. 6. Rotor angular velocity curves of each generator in different power systems. (a) Traditional power system. (b) Power system with integration of WTs.

On the one hand, since the equivalent inertia constant of WTs is much lower than that of synchronous generators, integrating them into the system reduces the relevant inertia coefficient in the coherency grouping model [30]. This change in inertia subsequently affects the clustering results. On the other hand, the PLL dynamics of DFIGs will affect its synchronous power, which in turn alters the original clustering characteristics of generator units. Consequently, the impact of integration of WTs on coherent clustering must be taken into account.

In order to validate the accuracy of the coherency grouping model with different types of integration of WTs, buses 10, 12, and 25 are replaced by WT3, WT3, and WT4 models with equivalent generation capacity, respectively, and other settings are in line with the above conditions. The results obtained by the coherency grouping model and the Fourier analysis are the same, both identified as {G1-G14}, {G15}, {G16-G19}, confirming the accuracy and reliability of the coherency grouping model with different types of integration of WTs.

B. Cluster Partitioning Solution

To assess the effect of randomness of RES output on the cluster partitioning, the power system is clustered by traditional power flow and the cluster searching in this paper, respectively.

Considering traditional power flow, the cluster partitioning results are illustrated in Fig. 7(a), with the corresponding cluster boundaries shown as the solid red lines in Fig. 4. The power system is divided into three clusters, with the bridges identified as {77-82, 80-96, 80-97, 80-99, 98-100, 85-86}, amounting to six lines.

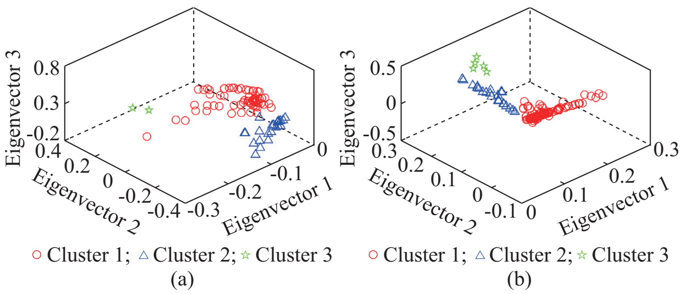

Fig. 7. Cluster partitioning results. (a) Considering traditional power flow. (b) Considering stochastic power flow.

Figure 7(b) presents the cluster partitioning results considering stochastic power flow, with the clustering results marked by the dashed red lines in Fig. 4. The power system is divided into three clusters with the bridges identified as {77-82, 80-96, 80-97, 80-99, 98-100, 82-83, 89-85, 89-88}, totaling eight transmission lines. While four bridges are in common compared with the traditional power flow, some discrepancies remain between the results.

To verify the advantages of the modified FCM clustering algorithm, the mapped spectral space dataset of IEEE 118-bus system is clustered using the traditional and modified FCM clustering algorithms, respectively. The comparison of clustering effects using the two algorithms is shown in Fig. 8.

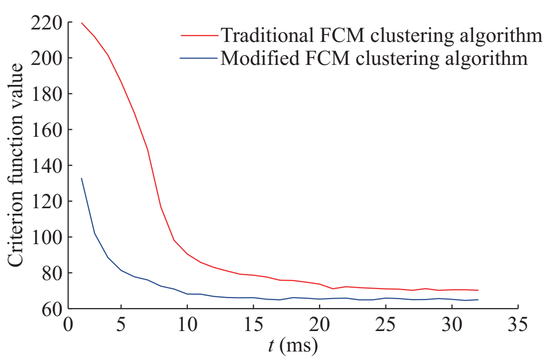

Fig. 8. Comparison of clustering effects using different algorithms.

The computational time of the modified and traditional FCM clustering algorithms are 12 ms and 24 ms, respectively. The obtained criterion function values of the modified and traditional FCM clustering algorithms are 66.2 and 70.8, respectively. The results show that the modified FCM clustering algorithm in this paper can effectively improve the clustering quality and computational efficiency.

In order to verify the necessity of considering stochastic power flow, the typical scenario generation method [31] is employed for comparison. A total of 1000 WT output scenarios, generated based on the Weibull distribution, are reduced to four representative scenarios. All other case settings remain consistent with those in Section V-A. The system is divided into three clusters, with the bridge selection range identified as {77-82, 77-80, 79-80, 80-81, 82-83, 89-92, 89-90}.

The typical scenario generation method derives representative WT output scenarios and their associated probabilities using sampled data. It emphasizes grouping generators according to different WT output patterns and identifying the corresponding separation points. In order to construct typical scenarios, the final separation section is determined using the inter-group distance index. This process involves a high computational cost, requiring 5.21 s to complete. By solving the stochastic power flow to determine the expected value of line active power, the cluster searching in this paper accounts for the uncertainties in RES output and load demand during the cluster partitioning analysis. The total computational time is 2.87 s, which is significantly shorter than that of the typical scenario method, demonstrating the superior efficiency of the cluster searching in this paper.

When considering stochastic power flow, the optimal range of bridges for the power system is shown in Fig. 9, including eight lines and three clusters.

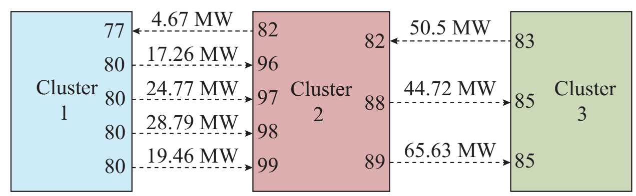

Fig. 9. Optimal range of bridges considering stochastic power flow.

The optimal bridges are selected based on the modified Prim's algorithm. Among the five bridges connecting Clusters 1 and 2, the line with the highest transmission power (28.79 MW on line 80-98) is chosen as the starting edge of the maximum spanning tree. Similarly, among the three bridges between Clusters 2 and 3, the line with the highest transmission power (65.63 MW on line 89-85) is selected as the maximum weight edge. At this point, the maximum spanning tree has included all the vertices. The result of optimal bridges considering stochastic power flow is shown in Fig. 10, and the total power disconnected in bridges is $(4.67+17.26+24.77+19.46)+(50.05+44.72)=160.93$ MW. Due to the unbalanced power flow p' between clusters is $[85.61, -25.31, -603]^{\mathrm{T}}$, the power flow in optimal bridges f' is $[85.61, 60.3]^{\mathrm{T}}$.

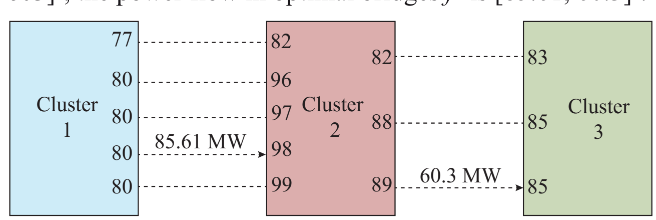

Fig. 10. Result of optimal bridges considering stochastic power flow.

By applying the tree-partitioning method, the generators considering integration of WTs are distributed across different partitions. The tree-partitioning method minimizes the power flow surge on transmission lines, in accordance with the principle of minimizing the line impact. Additionally, the power flow imbalance between clusters remains consistent with the pre-partitioning state, promoting safer and more stable operation of the power system. As the network connection between the clusters remains intact, synchronization during the recovery process is unnecessary, which significantly shortens the recovery time from cascading failures.

C. Results of Power Adjustment Measure

After selecting the optimal bridges, the non-optimal bridges between clusters are disconnected. Necessary adjustments to generator and load nodes within each cluster, in response to disconnected lines (77-82, 80-97, 80-99, 98-100, 82-83, and 89-85) and transmission lines with reduced power flow (e. g., 89-88), can be computed using the power adjustment measure. Power adjustment for the optimal bridge 80-98, where power flow increases, is taken using the method described in [32], ultimately resulting in the proposed strategy and adjustment values. The results of power adjustment measure are detailed in Table I.

TABLE I
RESULTS OF POWER ADJUSTMENT MEASURE

Cluster number	Controlled node	Control quantity (MW)	Total control quantity (MW)
Cluster 1	Load node 77	4.67	122.98
	Generator node 69	61.49	
	Generator node 80	56.82	
Cluster 2	Load node 82	12.69	109.44
	Load node 96	27.03	
	Load node 97	15.00	
	Generator node 89	5.33	
	Generator node 100	49.39	
Cluster 3	Load node 84	5.33	100.10
	Load node 85	24.00	
	Load node 86	20.72	
	Generator node 87	50.05	

Currently, some studies have employed data-driven methods to predict the likelihood of WT faults, with the goal of assisting in the risk evaluation of cascading failures [33]. Based on the situation awareness method for cascading failures [16], the failure scenarios with and without the proposed strategy are evaluated to verify the effectiveness of the proposed strategy for mitigating cascading failures [34]. The continuous time calculation of the proposed strategy is carried out, and the computational time is 11.86 s. Without relying on actual measurement data, the proposed strategy in this paper can meet the time requirements for emergency control.

The system failure scenario is defined as: at $t=40$ s, the active power of nodes 35, 40, and 42 is increased to 66 MW, 132 MW, and 192 MW (two times the original power), respectively. The loads at all other nodes remain unchanged, resulting in an increase of the total system load of 195 MW. An instantaneous three-phase-to-ground circuit is assumed to occur on lines 38-65 and 46-45 due to overload at $t=50$ s. The fault is cleared after 0.2 s. The active power of nodes 35, 40, and 42 is restored to 33 MW, 66 MW, and 96 MW at $t=55$ s, respectively. The rate of change in the average fault severity index for nodes 35, 40, and 42 at $t=40$ s is used as the threshold for the changing rate of fault severity index of the overall power system. The proposed strategy is triggered when the infection density of node surpasses 0.6. The infection densities of all nodes with and without the proposed strategy are shown in Fig. 11.

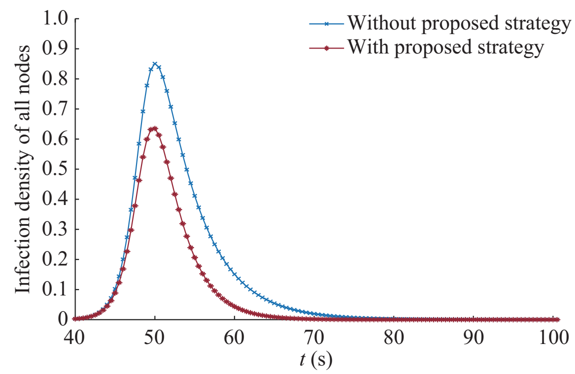

Fig. 11. Infection densities of all nodes with and without proposed strategy.

After implementing the proposed strategy, the maximum infected density peak (MIDP) is reduced to 0.6351, a significant decrease from the uncontrolled MIDP of 0.8505. The MIDP clearly demonstrates that early before the cascading failures expand further, applying the proposed strategy can significantly reduce the risk of fault propagation.

To emphasize the benefits of the proposed strategy, it is compared with two other strategies presented in [35] and [36], both of which employ active splitting. In order to illustrate the control effect on unbalanced power flow of the power system as well as the power distribution of bridges, the strategies presented in [35] and [36] along with the proposed strategy in this paper are referred to as strategies A, B, and C, respectively. The results of cluster partitioning are shown in Fig. 12(a) and (b).

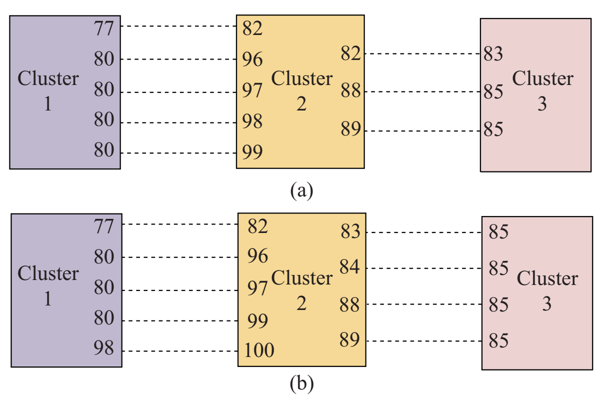

Fig. 12. Results of cluster partitioning. (a) Strategy A. (b) Strategy B.

Based on the principle of selecting the optimal bridge, the results of unbalanced power of the power system and the power of bridges for different strategies are shown in Table II.

TABLE II
UNBALANCED POWER OF POWER SYSTEM AND POWER OF BRIDGES FOR DIFFERENT STRATEGIES

Strategy	Disconnected line	Unbalanced power of power system (MW)	Proportion of unbalanced power (%)	Power of bridges (MW)
A	77-82, 80-96, 80-97, 80-98, 80-99, 82-83, 88-85, 89-85	492.02	11.21	0.00
B	77-82, 80-96, 80-97, 80-99, 98-100, 83-85, 84-85, 88-85, 89-85	487.66	11.11	0.00
C	77-82, 80-96, 80-97, 80-99, 82-83, 88-85	0.00	0.00	145.91

As for strategies A and B, the system is divided into separate islands that operate independently, with all bridges disconnected, leading to a high proportion of unbalanced power of the power system. The unbalanced power of the entire power system in strategies A and B represents 11.21% and 11.11% of the total system power, respectively. As for strategy C, the tree-partitioning method maintains the connection between clusters by enforcing a constraint during the implementation stage, ensuring that the power imbalance between clusters remains constant.

The cascading failure recovery process and recovery time are detailed in [16]. Table III presents the costs and recovery time for different strategies. As shown in Table III, strategy C achieves a significantly lower total control cost and shorter recovery time compared with strategies A and B, both of which use the traditional active splitting.

TABLE III
COMPARISON OF COSTS AND RECOVERY TIME OF DIFFERENT STRATEGIES

Strategy	Generator dispatch control cost ($)	Generator curtailment cost ($)	Load shedding cost ($)	Total control cost ($)	Recovery time (min)
A	0.00	7660.5	25535	33195.50	106
B	0.00	7920.0	26400	34320.00	113
C	113.64	4993.2	10962	16068.84	49

Due to the disconnection of all lines between the isolated islands, traditional strategies cause severe disturbances in line power flow (255.35 MW in strategy A and 264 MW in strategy B), while failing to balance the power among islands. Consequently, extensive generator and load adjustments are required, leading to additional economic losses. The total control costs of strategies A and B are higher than that of strategy C. Furthermore, strategies A and B result in more overloaded lines compared with strategy C. In strategy A, line 80-81 is severely overloaded, carrying 16 times its normal capacity, which leads to the unsafe operation of cluster 1. By contrast, in the three clusters obtained through strategy C, only a few lines experience mild overloads, which can be resolved through the power adjustment measure.

When strategies A and B are applied, all islands must be synchronized before reconnecting to the main grid, which significantly increases the recovery time and black-start costs. The total recovery time of strategies A and B is 57 min and 64 min longer than that of strategy C, respectively. In contrast, strategy C maintains the unbalanced power between clusters, and each cluster keeps its bridge connections to ensure that the power of bridges is unchanged. Changing the internal topology of the cluster only affects its internal power, without influencing the power of other clusters. From a power balance perspective, local faults within a cluster do not propagate to adjacent clusters through the bridges. Therefore, the proposed strategy can achieve local control of cascading failures with a lower total control cost and shorter recovery time.

D. Test on Actual Case System

To further demonstrate the effectiveness of the proposed strategy, an actual case system selected from the power system in a certain province of China is used for simulation. The total output power of grid-connected generators and the total system load is 56050.44 MW and 33521.81 MW, respectively. As shown in Supplementary Material A Fig. A1, there are 378 buses and 709 lines at voltages of 220 kV and above, of which nodes HZHW, YW, QJDC, XLT, XJH, JHA, and JHB are replaced by DFIG with equal capacity. The penetration rate of wind power is about 6%. A three-phase-to-ground fault is applied at line HP-DL. After the fault occurs, the generator nodes DHQ, MWW, TB, HD, WLN, LD, GGQ, and some 220 kV generator nodes belong to one group, while the remaining generator nodes belong to another.

To compare the cost of active splitting and tree-partitioning, strategy A and strategy C (the proposed strategy) are used as representatives. Table IV presents the comparison results of these two strategies.

TABLE IV
COMPARISON RESULTS OF TWO STRATEGIES

Strategy	Generator dispatch control cost ($)	Generator curtailment cost ($)	Load shedding cost ($)	Total control cost ($)	MIDP
A	0.00	54398.10	181327	235725.10	0.4457
C	2697.24	1298.62	129862	133757.86	0.3798

As shown in Table IV, strategy C reduces the total control cost by 43.26% compared with strategy A, and the MIDP after implementing strategy C is lower. The unbalanced power between clusters remains constant and all clusters continue to operate synchronously, and therefore, the required adjustments for generators and loads are smaller, resulting in fewer electrical disturbances. Changes in the internal topology of a cluster do not affect the power in other clusters, provided that inter-cluster power imbalances remain stable and the bridges between clusters are maintained. Thus, power fluctuations can be managed within each cluster, leading to a lower MIDP under strategy C. Moreover, strategy C has a continuous calculation time of 40.11 s in the actual case system, which can meet the time requirements for emergency control in large-scale power systems.

These results further confirm that the proposed strategy can achieve local management of cascading failures with lower total control cost and shorter recovery time.

VI. Conclusion

This paper proposes a novel tree-partitioning based emergency control strategy for mitigating cascading failures in power systems with integration of WTs.

1) The proposed strategy investigates the impact of integration of WTs on the identification of generator clusters. An improved phase motion equation is formulated for the coherency identification of both synchronous generators and DFIGs. The traditional line power flow is replaced with the expected value of stochastic power flow, thereby accounting for the variability introduced by WTs in power flow calculations. Under the ML and CL constraint pairs, the cluster searching in this paper produces cluster divisions that represent the behavior of power systems more accurately with high integration of WTs.

2) The proposed strategy can help reduce the risk of cascading failures and shorten the recovery time. The optimal bridges are selected using the modified Prim's algorithm, ensuring that clusters maintain the minimal connections and the number of disconnected lines is minimized. The application of tree-partitioning method helps reduce disturbances in power flow and further enhances the system stability. Additionally, during fault recovery, synchronization operations are not required, making the process more favorable for black-start conditions.

3) The proposed strategy can mitigate cascading failures with lower control costs. By maintaining a constant unbalanced power distribution between clusters, faults are confined within individual clusters. The proposed strategy quickly determines the adjustment range, targets, sequence, and magnitude of power adjustments for each cluster, ensuring safe and stable operation after control. Numerical results from both the IEEE 118-bus system and the actual case system confirm the effectiveness of the proposed strategy.

Current research primarily focuses on analyzing the effectiveness of emergency control strategies. Future studies could explore improvements in their efficiency and robustness with high penetration of RESs.

References

[1] H. Sun, B. Wang, W. Li *et al.*, "Analysis of cascading failure differences between traditional AC power grid and high-proportion new energy power grid," *Power System Technology*, vol. 45, no. 12, pp. 4641-4649, May 2021.

[2] S. Hashemi, B. Venkatasubramanian, P. Mancarella *et al.*, "Cascading-driven intentional controlled islanding for enhancing power grid operational resilience," *Journal of Modern Power Systems and Clean Energy*, vol. 14, no. 2, pp. 514-528, Mar. 2026

[3] I. Ngamroo, T. Surinkaew, and Y. Mitani, "Intelligence-driven grid-forming converter control for islanding microgrids," *Journal of Modern Power Systems and Clean Energy*, vol. 13, no. 4, pp. 1310-1322, Jul. 2025.

[4] B. Yang, V. Vittal, and G. Heydt, "Slow-coherency-based controlled islanding – a demonstration of the approach on the August 14, 2003 blackout scenario," *IEEE Transactions on Power Systems*, vol. 21, no. 4, pp. 1840-1847, Oct. 2006.

[5] T. Wang, Y. Liu, X. Gu *et al.*, "Vulnerable lines identification of power grid based on cascading fault space-time graph," *Proceedings of the CSEE*, vol. 39, no. 20, pp. 5962-5972, Oct. 2019.

[6] Y. Zhou, W. Hu, Y. Min *et al.*, "Active splitting strategy searching approach based on MISOCP with consideration of power island stability," *Journal of Modern Power Systems and Clean Energy*, vol. 7, no. 3, pp. 475-490, May 2019.

[7] M. Oboudi, M. Mohammadi, and M. Rastegar, "Resilience-oriented intentional islanding of reconfigurable distribution power systems," *Journal of Modern Power Systems and Clean Energy*, vol. 7, no. 4, pp. 741-752, Jul. 2019.

[8] T. Liu, J. Fu, C. He *et al.*, "Optimal controlled islanding strategy considering primary frequency response and uncertain renewable energy," *Proceedings of the CSEE*, vol. 43, no. 12, pp. 4568-4581, Jun. 2023.

[9] J. Li, C. Liu, and K. Schneider, "Controlled partitioning of a power network considering real and reactive power balance," *IEEE Transactions on Smart Grid*, vol. 1, no. 3, pp. 261-269, Nov. 2010.

[10] F. Teymouri, T. Amraee, H. Haberi *et al.*, "Toward controlled islanding for enhancing power grid resilience considering frequency stability constraints," *IEEE Transactions on Smart Grid*, vol. 10, no. 2, pp. 1735-1746, Nov. 2017.

[11] J. Bialek and V. Vahidinasab, "Tree-partitioning as an emergency measure to contain cascading line failures," *IEEE Transactions on Power Systems*, vol. 37, no. 1, pp. 467-475, Jun. 2021.

[12] J. Liu, F. Tang, J. Zhao *et al.*, "Coherency identification for wind-integrated power system using virtual synchronous motion equation," *IEEE Transactions on Power Systems*, vol. 35, no. 4, pp. 2619-2630, Jan. 2020.

[13] L. Ding, F. Gonzalez-Longatt, P. Wall *et al.*, "Two-step spectral clustering controlled islanding algorithm," *IEEE Transactions on Power Systems*, vol. 28, no. 1, pp. 75-84, Jun. 2012.

[14] G. Li, Z. Zhang, D. Li *et al.*, "Coherency clustering method based on Prony analysis feature extraction," *Power System Protection and Control*, vol. 48, no. 22, pp. 91-99, Nov. 2020.

[15] X. Wang, L. Ding, Z. Ma *et al.*, "Perturbation-based sensitivity analysis of slow coherency with variable power system inertia," *IEEE Transactions on Power Systems*, vol. 36, no. 2, pp. 1121-1129, Mar. 2021.

[16] J. Xu, Z. He, S. Liao *et al.*, "A detection method for cascading failure of power systems based on epidemic model," *CSEE Journal of Power and Energy Systems*, vol. 10. no. 3, pp. 1356-1370, Feb. 2024.

[17] M. Cheng, W. Yang, F. Wen *et al.*, "Controlled splitting sections searching method and islanding adjustment strategy for power system," *Automation of Electric Power Systems*, vol. 41, no. 19, pp. 37-45, Oct. 2017.

[18] Y. Huang, Q. Xu, H. Bian *et al.*, "Cumulant method based on Latin hypercube sampling for calculating probabilistic power flow," *Electric Power Automation Equipment*, vol. 36, no. 11, pp. 112-119, Nov. 2016.

[19] L. Dong, Y. Yang, C. Zhang *et al.*, "Probabilistic load flow considering network configuration uncertainties," *Transactions of China Electrotechnical Society*, vol. 27, no. 1, pp. 210-216, Jan. 2012.

[20] V. Luxburg, "A tutorial on spectral clustering," *Statistics and Computing*, vol. 17, no. 4, pp. 395-416, Aug. 2007.

[21] G. Chao, S. Sun, and J. Bi, "A survey on multiview clustering," *IEEE Transactions on Artificial Intelligence*, vol. 2, no, 2, pp. 146-168, Apr. 2021.

[22] Z. Wang, M. Zhang, H. Du *et al.*, "A searching algorithm for optimal controlled islanding surfaces considering VSC-HVDC terminal constraint," *Transactions of China Electrotechnical Society*, vol. 32, no.

17, pp. 57-66, Sept. 2017.
[23] L. Guo, C. Liang, and S. Low, "Monotonicity properties and spectral characterization of power redistribution in cascading failures," *ACM SIGMETRICS Performance Evaluation Review*, vol. 45, no. 2, pp. 103-106, Oct. 2017.
[24] L. Guo, C. Liang, A. Zocca *et al*., "Failure localization in power systems via tree partitions," *ACM SIGMETRICS Performance Evaluation Review*, vol. 46, no. 2, pp. 57-61, Jan. 2019.
[25] X. Dong and Y. Lu, "Islanding algorithm for distributed generators based on improved Prim algorithm," *Power System Technology*, vol. 34, no. 9, pp. 195-201, Sept. 2010.
[26] M. Rao, S. Soman, P. Chitkara *et al*., "Min-max fair power flow tracing for transmission system usage cost allocation: a large system perspective," *IEEE Transactions on Power Systems*, vol. 25, no. 3, pp. 1457-1468, Feb. 2010.
[27] Y. Wu, T. Wang, H. Fan *et al*., "Blocking control of cascading failure for large-scale wind power systems system using sensitivity analysis," *Power System Technology*, vol. 47, no. 9, pp. 3743-3755, Sept. 2023.
[28] M. Jonsson, M. Begovic, and J. Daalder, "A new method suitable for real-time generator coherency determination," *IEEE Transactions on Power Systems*, vol. 19, no. 3, pp. 1473-1482, Aug. 2004.
[29] Z. Wang, M. Zhang, H. Du *et al*., "A searching algorithm for optimal controlled islanding surfaces considering VSC-HVDC terminal constraint," *Transactions of China Electrotechnical Society*, vol. 32, no. 17, pp. 57-66, Sept. 2017.
[30] Q. Xing, T. Wang, and S. Huang, "On-line identification of equivalent inertia for DFIG wind turbines based on extended Kalman filter," in *Proceedings of 2021 IEEE/IAS Industrial and Commercial Power System Asia*, Chengdu, China, Jul. 2021, pp. 18-21.
[31] L. Liu, "Identification of power system unit coherence and active separation section search under wind farm connection," M.S. dissertation, Xi'an University of Technology, Xi'an, China, 2024.
[32] K. Zeng, J. Wen, S. Cheng *et al*., "Critical line identification of complex power system in cascading failure," *Proceedings of the CSEE*, vol. 34, no. 7, pp. 1103-1111, Mar. 2014.
[33] A. Wan, W. Gong, A. Khalil *et al*., "Data-driven early fire detection in offshore wind turbines: a TCN-ECA based approach leveraging SCADA data," *Process Safety and Environmental Protection*, vol. 20, p. 107373, Aug. 2025.
[34] K. Sun, D. Zheng, and Q. Lu, "A simulation study of OBDD-based proper splitting strategies for power systems under consideration of transient stability," *IEEE Transactions on Power Systems*, vol. 20, no. 1. pp. 389-399, Feb. 2005.
[35] C. Wang, B. Zhang, Z. Hao *et al*., "A real-time searching method for splitting surfaces of the power system," *Proceedings of the CSEE*, vol. 30, no. 7, pp. 48-55, Mar. 2010.
[36] Z. Pan and Y. Zhang, "A flexible black-start network partitioning strategy considering subsystem recovery time balance," *International Transactions on Electrical Energy Systems*, vol. 25, no. 8, pp. 1644-1656, Aug. 2015.

Jian Xu received the B.S. and Ph.D. degrees in electrical engineering from Wuhan University, Wuhan, China, in 2002 and 2007, respectively. He is currently a Professor with the School of Electrical Engineering and Automation, Wuhan University. His research interests include power system operation, voltage stability, and wind power control and integration.

Zhonghao He received the B.S degree in electrical engineering and automation from North China Electric Power University, Beijing, China, in 2017. He is currently pursuing the Ph.D. degree in civil and hydraulic engineering at the School of Electrical Engineering and Automation, Wuhan University, Wuhan, China. He is also an Engineer with Yichang Power Supply Company, State Grid Hubei Electric Power Company, Yichang, China. His research interests include power system reliability and cascading failure.

Longwen Jia received the B.S. degree in smart grid information engineering from North China Electric Power University, Beijing, China, in 2022. He is currently working towards the Ph.D. degree at the School of Electrical Engineering and Automation, Wuhan University, Wuhan, China. His research interests include power system operation and computational intelligence.

Siyang Liao received the B.S. and Ph.D. degrees in electrical engineering from Wuhan University, Wuhan, China, in 2011 and 2016, respectively. He is currently an Associated Professor with the School of Electrical Engineering and Automation, Wuhan University. His research interests include wind power integration and power system simulation.

Yaokun Zou received the B.S degree from College of Electrical Engineering, Sichuan University, Chengdu, China, in 2020. He is currently pursuing the Ph.D. degree in electrical engineering at the School of Electrical Engineering and Automation, Wuhan University, Wuhan, China. His research interests include energy management and operation control of power system.